

# Effects of Tungsten Fiber on Failure Mode of Zr-Based Bulk Metallic Glassy Composite

H. ZHANG, Z.F. ZHANG, Z.G. WANG, K.Q. QIU, H.F. ZHANG, and Q.S. ZANG

The authors systematically investigated the effects of tungsten fiber on failure mode as well as deformation and fracture mechanisms in tungsten fiber-reinforced  $Zr_{41.25}Ti_{13.75}Ni_{10}Cu_{12.5}Be_{22.5}$  bulk metallic glassy composite under uniaxial compression at room and high temperatures. At room temperature, the failure mode of the composite changes from shear fracture to longitudinal splitting failure with increasing fiber volume fraction. Similar to the observations in monolithic metallic glasses, the shear fracture angle of the composite is approximately equal to  $39\sim 40$  deg, indicating that the Mohr-Coulomb criterion is suitable to give the critical shear fracture condition of the composite. When the compression tests were performed below the glass transition temperature of  $Zr_{41.25}Ti_{13.75}Ni_{10}Cu_{12.5}Be_{22.5}$  metallic glass  $T_g$ , the deformation behavior of the composite strongly depends on the strain rates and the test temperature, which is quite similar to the deformation behavior of monolithic metallic glasses in the supercooled liquid region. The corresponding failure mode of the composite changes from shear or splitting fracture to bending failure with decreasing strain rate or increasing test temperature. The failure modes at the temperature near  $T_g$  are mainly controlled by the metallic glass matrix due to the decrease in its viscosity at high temperature. Based on these multiple failure modes, the effects of test temperature and tungsten fiber volume fraction on deformation and fracture mechanisms are summarized.

## I. INTRODUCTION

BULK metallic glasses (BMGs) have gained considerable attention as potential structural materials for engineering application in recent years. In comparison with crystalline metals or alloys, which have been extensively used in many areas, metallic glasses possess some exceptional mechanical properties—*i.e.*, high tensile and compressive strength, good elasticity and excellent physical and chemical properties.<sup>[1,2]</sup> Recent studies have revealed some interesting mechanical properties of BMGs. Inoue *et al.* found that Co-based BMG has a very high fracture strength of over 5000 MPa.<sup>[3]</sup> Fracture toughness of some BMGs is much higher than that of brittle ceramics and is generally in the range of 18 to 70 MPa  $\sqrt{m}$ , which is comparable to that of polycrystalline metals or alloys.<sup>[4,5,6]</sup> BMGs are susceptible to fatigue degradation with fatigue exponent  $m$  of 1  $\sim$  2 in the Paris power law relationship.<sup>[7,8,9]</sup> Among the several families of multicomponent metallic glasses, Zr-based metallic glasses have exhibited exceptional glass-forming ability with a low critical cooling rate and a wide supercooled liquid region.<sup>[10,11]</sup>

Extensive studies have established that BMGs always fail with very little plasticity at room temperature under both tension and compression due to the formation of highly localized shear bands.<sup>[12,13]</sup> Therefore, many efforts have been devoted to improve the plasticity of BMGs while keeping high strength through processing BMG matrix composites.<sup>[14,15]</sup> Obviously improved mechanical properties have been obtained in a series of Zr- and Ti-based metallic glass

matrix or ultra-fine-structured matrix composites.<sup>[16,17,18]</sup> Plastic strain as high as 30 pct and fracture stress of  $\sim 2$  GPa have been observed in an *in situ* formed Ti-based composite containing ductile dendritic phase and nanostructured matrix synthesized by copper mold casting or arc-melting method.<sup>[14,18,19]</sup> The enhanced ductility has been shown to originate from the strong interactions of the shear bands in the glassy matrix with the dendritic phases.<sup>[19,20]</sup>

Besides the dendrite-reinforced composites, tungsten fiber has been regarded as another reinforcement for BMG composite that exhibited enhanced mechanical properties under quasi-static or dynamic deformation.<sup>[21,22,23]</sup> Both compressive plastic strain to failure and fracture strength have been improved in such BMG composite.<sup>[21]</sup> Ballistic tests by firing tungsten fiber composite rods into aluminum and steel targets have indicated that shear deformation is the main failure mode at very high strain rates.<sup>[24]</sup>

Up to now, a limited amount of preliminary work has been conducted on the mechanical properties of tungsten fiber-reinforced BMG composite. Thus, it is necessary to seek a better understanding of the deformation and fracture behavior for such composite. We conducted a comprehensive study on the deformation and fracture behavior of tungsten fiber-reinforced  $Zr_{41.25}Ti_{13.75}Ni_{10}Cu_{12.5}Be_{22.5}$  composite under compression at room or high temperature to reveal the predominant mechanisms controlling various fracture modes in this composite.

## II. MATERIAL AND EXPERIMENTAL PROCEDURES

Ingots of  $Zr_{41.25}Ti_{13.75}Ni_{10}Cu_{12.5}Be_{22.5}$  (in at. pct) were first prepared by combining the constitutive elements (purity 99.5 pct or higher) in an induction furnace under an argon atmosphere. Tungsten fibers with nominal diameter of  $\sim 300$   $\mu\text{m}$  were straightened and cut into 80 mm in length. The fibers were cleaned in a bath of acetone through an

H. ZHANG, Associate Professor, Z.F. ZHANG, Professor, Z.G. WANG, Professor, H.F. ZHANG, Professor, and Q.S. ZANG, Professor, are with the Shenyang National Laboratory for Materials Science, Institute of Metal Research, Chinese Academy of Sciences, 110016 Shenyang, People's Republic of China. Contact e-mail: zhzhzhang@imr.ac.cn K.Q. QIU, Professor, is with the School of Materials Science and Engineering, Shenyang University of Technology, 110023 Shenyang, People's Republic of China.

Manuscript submitted May 13, 2005.

ultrasonic method and then cleaned by ethanol. Typical mechanical properties of the tungsten fiber and metallic glass  $Zr_{41.25}Ti_{13.75}Ni_{10}Cu_{12.5}Be_{22.5}$  are listed in Table I. The tungsten fibers were placed in the sealed end of an evacuated quartz tube. The ingots were then heated and melted in a resistive furnace, followed by pressure infiltration. The sample tube was then quenched in a supersaturated brine solution. Details of the casting process are described elsewhere.<sup>[25,26]</sup>

Cross-section of the tungsten/ $Zr_{41.25}Ti_{13.75}Ni_{10}Cu_{12.5}Be_{22.5}$  composite was observed by a Cambridge S360 scanning electron microscope (SEM) in a backscatter mode (Figure 1). Similar to some other tungsten fiber-reinforced  $Zr_{41.25}Ti_{13.75}Ni_{10}Cu_{12.5}Be_{22.5}$  metallic glass composites,<sup>[25]</sup> the interfacial crystals between the fiber and the glassy matrix are rare in the present material. Metallic glass  $Zr_{41.25}Ti_{13.75}Ni_{10}Cu_{12.5}Be_{22.5}$  and its tungsten fiber composites with different tungsten fiber volume fraction were cut into a dimension of 3 mm × 3 mm × 6 mm by wire electrical discharge machining. The surfaces of the specimen were mechanically polished before testing. Room-temperature compression tests were conducted on a computer-controlled, servo-hydraulic MTS 810 testing machine using displacement control (strain rate of  $1 \times 10^{-3} \text{ s}^{-1}$ ). The loading axis is parallel to the fiber direction. High-temperature compression tests were conducted using a Schenck testing machine equipped with a temperature-controlled air furnace. Two strain rates,  $1 \times 10^{-3} \text{ s}^{-1}$  and  $1 \times 10^{-4} \text{ s}^{-1}$ , were selected for the high-temperature tests. The high-temperature tests were stopped when the composite fractured or failed in a bending or “barrelling” mode, which was indicated by a slow load drop with increasing the displacement. Side surface and fracture surface of the deformed composite specimens were subsequently examined using SEM.

**Table I. Selected Properties of the Tungsten Fiber and  $Zr_{41.25}Ti_{13.75}Ni_{10}Cu_{12.5}Be_{22.5}$  Metallic Glass**

Material	$Zr_{41.25}Ti_{13.75}Ni_{10}Cu_{12.5}Be_{22.5}$	Tungsten Fiber
Young's Modulus (GPa)	98	405
Ultimate Strength (MPa)	1800	2200
Poisson's Ratio	0.36	0.28

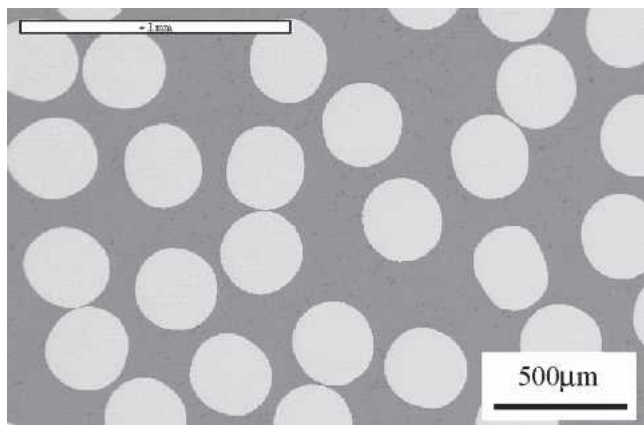


Fig. 1—Backscatter SEM micrograph of the tungsten fiber-reinforced  $Zr_{41.25}Ti_{13.75}Ni_{10}Cu_{12.5}Be_{22.5}$  metallic glassy composite.

### III. RESULTS

#### A. Compression Failure at Room Temperature

$Zr_{41.25}Ti_{13.75}Ni_{10}Cu_{12.5}Be_{22.5}$  metallic glass and its tungsten fiber composite specimens with different fiber volume fraction ( $V_f$ ) from 10 pct to 60 pct were selected for the compression test at room temperature. Typical compressive stress–strain curves of  $Zr_{41.25}Ti_{13.75}Ni_{10}Cu_{12.5}Be_{22.5}$  metallic glass and two composites with fiber volume fractions of 16 pct and 56 pct are shown in Figure 2. The fracture strength of  $Zr_{41.25}Ti_{13.75}Ni_{10}Cu_{12.5}Be_{22.5}$  metallic glass is about 1.8 GPa, and the fracture strength of the composites increases with increasing the fiber volume fraction. For the composite with 16 vol pct fiber, there is no plastic deformation, indicating that the addition of a few tungsten fibers has no obvious influence on the mechanical properties of the composite. When the fiber volume fraction is 56 pct, the composite specimen exhibits both high strength and large plastic strain to failure (more than 10 pct). This is in contrast to monolithic BMGs, which usually fail with little or no plasticity.<sup>[13,27]</sup> Similar to the elastic-perfectly-plastic behavior usually observed in monolithic metallic glasses under compression, no work hardening can be observed for the composite with high fiber volume fraction.

For  $Zr_{41.25}Ti_{13.75}Ni_{10}Cu_{12.5}Be_{22.5}$  metallic glass and the composite with 16 vol pct tungsten fiber, their fracture was observed to occur in a shear mode. Similar to that in monolithic BMGs,<sup>[13,28–31]</sup> shear fracture angle  $\theta_C$  between the compressive axis and the fracture plane is smaller than 45 deg ( $\sim 40$  deg), as shown in Figures 3(a) and (b). Shear fracture of the two specimens does not proceed along the maximum shear stress plane under compression. This shear fracture behavior is consistent with the previous observations on some monolithic metallic glasses with a shear fracture angle smaller than 45 deg under compression.<sup>[13,28–31]</sup> In addition, multiple shear bands are observed to form in the metallic glass matrix surrounded by the tungsten fibers, as shown in Figure 3(c). Obviously, propagation of these shear bands is usually blocked by the neighboring tungsten fibers. Fiber/metallic glass interfacial debonding and longitudinal fiber splitting can also be observed, as shown in

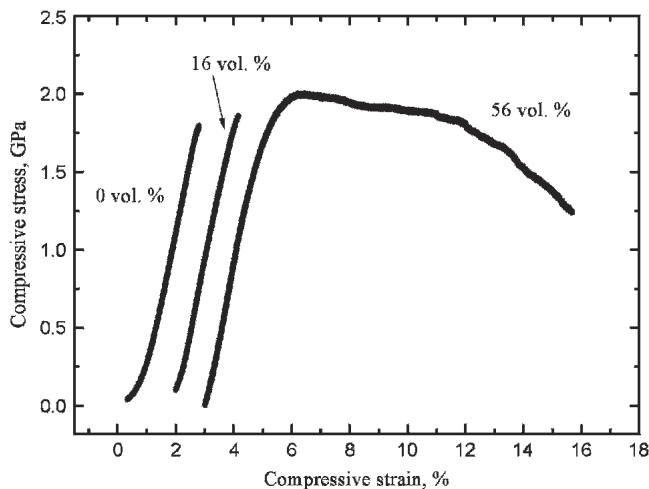


Fig. 2—Room-temperature compressive stress–strain curves of  $Zr_{41.25}Ti_{13.75}Ni_{10}Cu_{12.5}Be_{22.5}$  metallic glass and its composites with different fiber volume fractions.

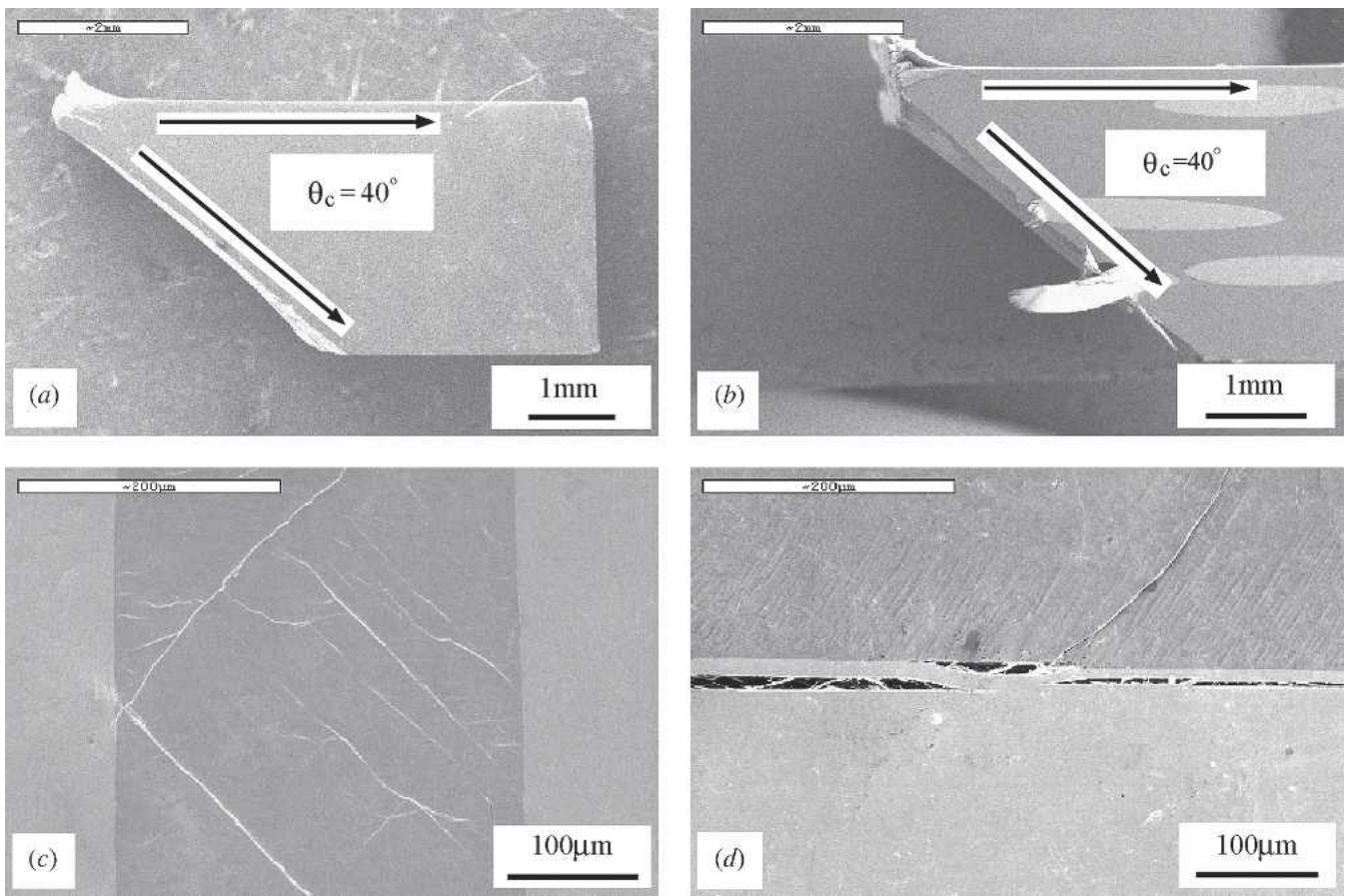


Fig. 3—SEM micrograph of the specimen surfaces in  $Zr_{41.25}Ti_{13.75}Ni_{10}Cu_{12.5}Be_{22.5}$  metallic glass and its tungsten fiber composite: (a) shear fracture of  $Zr_{41.25}Ti_{13.75}Ni_{10}Cu_{12.5}Be_{22.5}$ , (b) shear fracture of the 16 vol pct fiber composite, (c) multiple shear bands in the metallic glass matrix, (d) longitudinal splitting of the tungsten fiber and tungsten fiber/matrix interfacial debonding.

Figure 3(d). Moreover, fiber/metallic glass interfacial debonding was seldom observed due to the existence of a residual compressive stress at the interface.<sup>[21]</sup> These observations reveal that shear fracture is the main failure mode at room temperature for the composite containing few fibers.

Figure 4(a) shows the shear fracture surface morphology in the composite with 16 vol pct fiber. There exists fiber/matrix interfacial debonding at some tungsten fibers marked by A, whereas no such cracking can be observed at other tungsten fibers marked by B. At higher magnification, it can be clearly seen that the degree of the fiber/matrix interfacial debonding is not high after shear fracture (Figure 4(b)). Similar to the observations in Figures 3(c) and (d), this indicates a strong bonding of the fiber/metallic glass interface. Part of the fracture surface of the tungsten fiber is covered with a thin layer of the molten metallic glass, and a vein-like morphology appears on the fracture surface of the metallic glassy matrix, which is similar to that observed in some monolithic metallic glasses.<sup>[13,30–33]</sup> These observations indicate that the localized shear fracture of the tungsten composite leads to a concentrated release of the elastic energy stored during compression. Reduced viscosity or local melting may occur for the metallic glass at the moment of fracture due to rapid release of the elastic energy.<sup>[13,29]</sup>

Figure 5(a) shows the fracture surface of the composite specimen with 56 vol pct tungsten fiber. In contrast to shear

fracture mode in the 16 vol pct fiber composite, this specimen failed in a longitudinal splitting mode. Normally, the specimen tends to split into two parts along the loading axis. It has been observed that tungsten fiber-reinforced metallic glasses with high fiber volume fraction generally fractured in a longitudinal splitting mode.<sup>[21,26]</sup> Conner *et al.* and Qiu *et al.* found that the fracture mode of the tungsten composites changed to longitudinal splitting when the fiber volume fraction exceeded  $\sim 60$  pct.<sup>[21,26]</sup> These results demonstrate that the failure mode of the tungsten composite may change from shear fracture to splitting fracture with increasing fiber volume fraction. It is also observed from Figure 5(a) that the fracture of the composite resulted from debonding at the fiber/matrix interfaces or longitudinal splitting of the tungsten fibers. It has been pointed out that tensile matrix hoop stress may exist in the tungsten composite and may encourage cracks to propagate towards the reinforcing fibers,<sup>[21]</sup> leading to longitudinal splitting of the tungsten fiber under compression. Other fracture modes can also be observed in the 56 vol pct fiber composite. Figure 5(b) shows severe shear fracture occurring locally through one to two tungsten fibers. On the specimen surface, several sites of longitudinal splitting of a tungsten fiber can be observed, as shown in Figure 5(c). However, fiber/matrix interfacial debonding is seldom observed because of a strong bonding of the interface caused by the residual compressive stress. In addition,

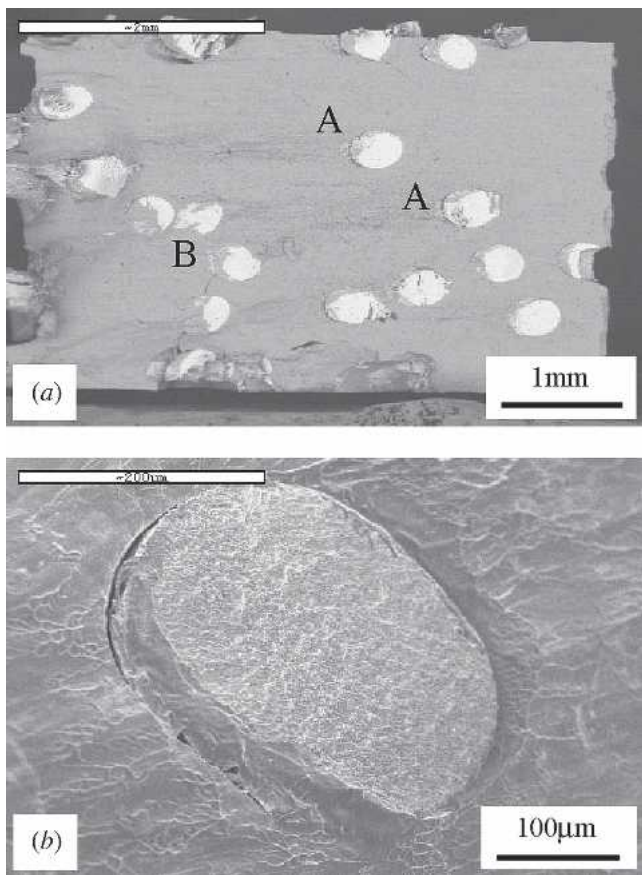


Fig. 4—SEM micrograph of the 16 vol pct tungsten fiber/ $Zr_{41.25}Ti_{13.75}Ni_{10}Cu_{12.5}Be_{22.5}$  composite: (a) shear fracture surface, (b) localized debonding at the tungsten fiber/matrix interface on the fracture surface. A thin layer of metallic glass formed on a tungsten fiber caused by reduced viscosity of the metallic glass during shear fracture.

multiple shear bands oriented at a direction smaller than 45 deg to the loading axis can be seen in the matrix, as shown in Figure 5(d). One of the shear bands may develop to a crack with increasing the compressive stress and continue to propagate in a shear mode. It is believed that the multiple shear bands and longitudinal cracking of the tungsten fibers may contribute to the enhanced plastic strain of the composite. These microscopically competitive processes may eventually lead to shear or splitting fracture of the composite.

#### B. Compression Failure at High Temperature

High-temperature compression tests of the tungsten composite were performed at some selected temperatures below the glass transition temperature of metallic glass  $Zr_{41.25}Ti_{13.75}Ni_{10}Cu_{12.5}Be_{22.5}$  ( $T_g = \sim 628$  K)<sup>[34,35]</sup> to reveal different failure modes of the composite. Two strain rates,  $1 \times 10^{-3} s^{-1}$  and  $1 \times 10^{-4} s^{-1}$ , were selected for the compression tests. The selected fiber volume fractions of the composite for the high-temperature test are in the range of 35~50 pct. Typical failure modes at different strain rates and temperatures are listed in Table II. It can be seen that the deformation behavior and fracture mode of the composite strongly depend on the strain rate and the test temperature. In a few cases, bending or “barrelling” deformation of the specimens can be seen at high temperatures.

Besides, it is observed that bending failure tends to occur at a lower strain rate at the same temperature. This strain rate-dependent behavior of deformation and failure has also been observed in some monolithic metallic glasses tested in the supercooled liquid region.<sup>[36,37]</sup> Figure 6(a) shows the shear fracture (shear fracture angle  $\theta_C = 39$  deg) of a 35 vol pct fiber composite tested at a strain rate of  $1 \times 10^{-4} s^{-1}$  and temperature of 543 K. It is noted that the shear fracture plane of the composite also deviates from the maximum shear stress plane (45 deg) at high temperature. The test was stopped immediately after the shear fracture of the specimen was detected from a load drop in the load–displacement curve. As shown in Figure 6(b), the primary shear band propagated in the matrix and terminated at a tungsten fiber, demonstrating a strong blocking effect of the tungsten fiber on shear fracture of the composite. The subsequent fracture of the composite is supposed to proceed either along the original shear band or along the fiber/matrix interface, as marked by the arrows in Figure 6(b). The final failure of the composite will strongly depend on the competitive processes between shear fracture and longitudinal splitting and will be discussed in the following sections.

The specimen with 48 vol pct fiber lost its parallelepiped shape and became bended when it was compressed at a strain rate of  $1 \times 10^{-4} s^{-1}$  and temperature of 563 K, as shown in Figure 6(c). Some specimens with high fiber volume fraction have been found to fail in a longitudinal splitting mode at higher strain rate, which is similar to the fracture mode of the high-fiber  $V_f$  specimen tested at room temperature. At a temperature near  $T_g$  (e.g., 628 K), specimen bending becomes the main failure mode irrespective of the applied strain rate, as shown in Figure 6(d). Therefore, failure modes of the composite at high temperatures strongly depend on the applied temperature, strain rate, and tungsten fiber volume fraction.

## IV. DISCUSSION

### A. Shear and Splitting Fracture Mechanisms at Room Temperature

It has been observed from this study that the failure modes at room temperature are quite different in the tungsten fiber/ $Zr_{41.25}Ti_{13.75}Ni_{10}Cu_{12.5}Be_{22.5}$  composite specimens with different fiber volume fractions. Shear fracture usually happens when the fiber volume fraction is low. The tungsten composite specimens generally fail in a longitudinal splitting mode when the fiber volume fraction exceeds  $\sim 60$  pct. This demonstrates that longitudinal splitting is the main failure mode for the specimen with high fiber volume fraction.

Shear fracture has been widely observed for many metallic glasses<sup>[13,28–31]</sup> and metallic glass composites.<sup>[14,18,19,33,38]</sup> Moreover, metallic glass and its composite usually fail in a shear mode under compression with shear fracture angle smaller than 45 deg, which deviates from the maximum shear stress plane.<sup>[28–31,33,38,39]</sup> For the 16 vol pct tungsten fiber composite, the compressive shear fracture angle  $\theta_C$  between the loading axis and the shear fracture plane is about 40 deg. A similar shear fracture angle has also been observed in other tungsten fiber composite specimens with different fiber volume fractions, as listed in Table II. It is found that shear fracture angles of the tungsten composites are about 39~40 deg irrespective of the fiber volume fraction. This

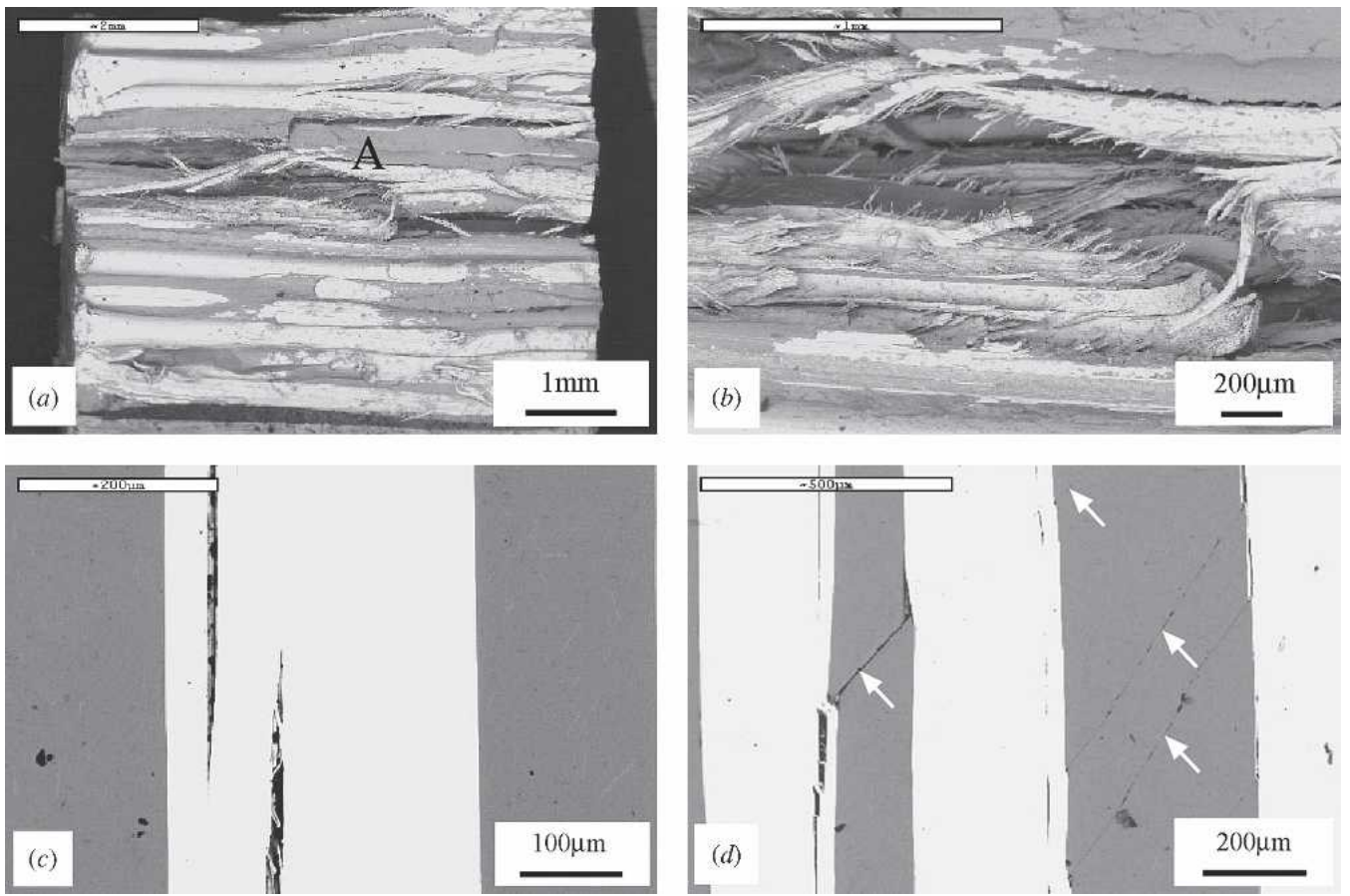


Fig. 5—SEM micrograph of the 56 vol pct tungsten fiber/ $Zr_{41.25}Ti_{13.75}Ni_{10}Cu_{12.5}Be_{22.5}$  composite: (a) fracture surface of the split composite specimen under compression, (b) a higher-magnification view of region A in (a), showing localized shear fracture through tungsten fibers, (c) longitudinal splitting in a tungsten fiber, (d) the competitive process between multiple shear bands in the metallic glass matrix (white arrows) and splitting in the tungsten fibers.

**Table II. Deformation Properties of the Composites at High Temperatures**

Strain Rate ( $s^{-1}$ )	Peak Stress (GPa)	Temperature (K)	Failure Mode	Fiber Volume Fraction
$1 \times 10^{-4}$	2.01	543	Shear fracture	35 pct
$1 \times 10^{-3}$	2.17	563	Longitudinal splitting	44 pct
$1 \times 10^{-4}$	2.18	563	Bending	48 pct
$1 \times 10^{-4}$	1.97	563	Bending	49 pct
$1 \times 10^{-4}$	1.98	583	Bending	46 pct
$1 \times 10^{-3}$	1.96	603	Longitudinal splitting	46 pct
$1 \times 10^{-3}$	2.07	603	Longitudinal splitting	49 pct
$1 \times 10^{-3}$	1.33	623	Bending	43 pct
$1 \times 10^{-3}$		623	Bending	38 pct

deviation of the shear fracture plane from the maximum shear stress plane also demonstrates that shear fracture of the tungsten composites does not follow Tresca criterion. The Mohr-Coulomb criterion has been used to explain the deviation from the maximum shear stress plane in monolithic metallic glasses by taking the normal stress into account.<sup>[28,31,33,40,41]</sup> For the tungsten composite in the current study, when shear stress on a plane reaches a critical value under compression, the specimen will fail in a shear mode with the shear fracture angle of  $\sim 40$  deg. This critical shear fracture condition can be expressed as:<sup>[28–31,33,40,41]</sup>

$$\tau_{\theta} = \tau_0 + \mu_0 \sigma_{\theta}, \quad [1]$$

where  $\tau_0$  is the critical shear strength on the shear fracture plane without normal stress;  $\mu_0$  is a constant of the material, indicating the effect of normal stress on the shear fracture plane; and  $\tau_{\theta}$  and  $\sigma_{\theta}$  are shear and normal stresses on the shear fracture plane.

According to the rule of mixtures in fiber-reinforced composite,  $\tau_0$  in Eq. (1) can be expressed as:

$$\tau_0 = \tau_m(1 - V_f) + \tau_f V_f, \quad [2]$$

where  $\tau_m$  and  $\tau_f$  are critical shear strengths on the shear fracture plane of the metallic glass matrix and the tungsten fiber, respectively. In addition, shear and normal stresses,  $\tau_{\theta}$  and  $\sigma_{\theta}$ , on the shear fracture plane of the composite can be written as:

$$\tau_{\theta} = \sigma_{shear} \sin \theta_C \cos \theta_C \quad [3a]$$

$$\sigma_{\theta} = \sigma_{shear} \sin^2 \theta_C, \quad [3b]$$

where  $\sigma_{shear}$  is the compressive fracture strength of the composite failed in a shear mode and  $\theta_C$  is the actual shear

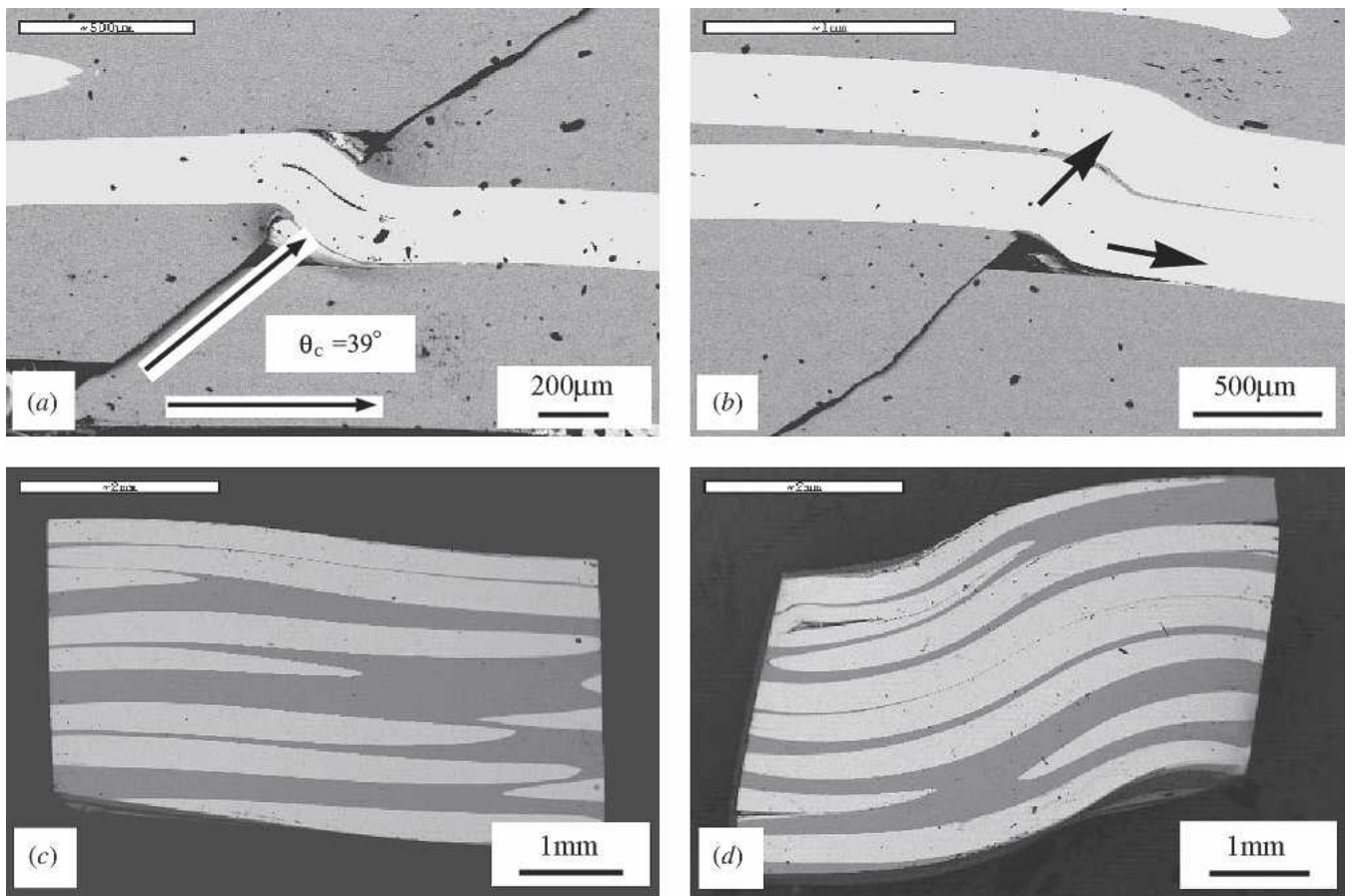


Fig. 6—SEM micrograph of the tungsten composite compressed at high temperatures: (a) localized shear fracture of a 35 vol pct tungsten composite at 543 K and a strain rate of  $1 \times 10^{-4} \text{ s}^{-1}$ , (b) propagation of the shear band is blocked by a tungsten fiber, (c) bending of a 48 vol pct composite specimen at 563 K and a strain rate of  $1 \times 10^{-4} \text{ s}^{-1}$ , (d) bending of a 43 vol pct composite specimen at 623 K and a strain rate of  $1 \times 10^{-3} \text{ s}^{-1}$ .

fracture angle. Substituting Eqs. [2], [3a], and [3b] into Eq. [1], one can get:

$$\sigma_{shear}(\sin \theta_C \cos \theta_C - \mu_0 \sin^2 \theta_C) = \tau_m(1 - V_f) + \tau_f V_f. \quad [4]$$

Therefore, the following relationship can be obtained:

$$\sigma_{shear} = k[\tau_m(1 - V_f) + \tau_f V_f], \quad [5]$$

with  $k$  a constant expressed as:

$$k = \frac{1}{\sin \theta_C \cos \theta_C - \mu_0 \sin^2 \theta_C}. \quad [6]$$

Since the fracture strength of the tungsten fiber is higher than that of  $\text{Zr}_{41.25}\text{Ti}_{13.75}\text{Ni}_{10}\text{Cu}_{12.5}\text{Be}_{22.5}$  metallic glass (Table I), critical shear strength  $\tau_f$  should be higher than  $\tau_m$ . Therefore, from Eq. [5], the compressive fracture strength  $\sigma_{shear}$  of the composite will increase with increasing fiber volume fraction, as schematically illustrated in Figure 7(a).

For the composite with a high fiber volume fraction, localized splitting of the tungsten fiber along the longitudinal direction can be found in some area of the specimen surface (Figure 5(c)). The composite will eventually fail in a splitting mode. On the other hand, multiple shear bands

can be observed in the metallic glassy matrix (Figure 5(d)). It is believed that these shear bands in the matrix will cause shear fracture of the specimen, whereas splitting of the fiber may lead to splitting failure of the specimen. Therefore, failure of the composite can be reflected microscopically by the competitive processes between shear band development in the matrix and splitting fracture of the tungsten fiber.

For a better understanding of the competitive processes between shear and splitting fracture of the composite, it is supposed that there exist critical shear fracture stresses on the shear fracture plane,  $\tau_{\theta}^{V_1}$  and  $\tau_{\theta}^{V_2}$ , for composites with fiber volume fraction of  $V_1$  pct and  $V_2$  pct, respectively.  $V_1$  pct and  $V_2$  pct stand for two composites with fiber volume fractions of 16 pct and 56 pct, respectively. According to the Mohr-Coulomb criterion,<sup>[30,31,33]</sup> shear fracture may occur for the two composites when the following conditions are satisfied:

$$\tau_{\theta}^{V_1} = \tau_0^{V_1} + \mu_0^{V_1} \sigma_{\theta}^{V_1} \quad (V_1 \text{ pct}) \quad [7a]$$

$$\tau_{\theta}^{V_2} = \tau_0^{V_2} + \mu_0^{V_2} \sigma_{\theta}^{V_2}, \quad (V_2 \text{ pct}) \quad [7b]$$

where constants  $\mu_0^{V_1}$  and  $\mu_0^{V_2}$  are functions of the shear fracture angle for the  $V_1$  pct and  $V_2$  pct fiber composites,

respectively. For the composites with different fiber volume fractions,  $\mu_0^{V_1}$  and  $\mu_0^{V_2}$  are almost equal because they have almost the same shear fracture angle of 39~40 deg (Table II)—*i.e.*,  $\mu_0^{V_1} = \mu_0^{V_2}$ .  $\tau_\theta^{V_1}$ ,  $\sigma_\theta^{V_1}$ ,  $\tau_\theta^{V_2}$ , and  $\sigma_\theta^{V_2}$  are shear and normal stresses on the shear fracture plane for the two composites.  $\tau_0^{V_1}$  and  $\tau_0^{V_2}$  are critical shear strengths on the shear fracture plane for the  $V_1$  pct and  $V_2$  pct composites, respectively. From Eq. [2],  $\tau_0$  increases with increasing fiber volume fraction. Therefore,  $\tau_0^{V_2}$  should be higher than  $\tau_0^{V_1}$ , *i.e.*,  $\tau_0^{V_2} > \tau_0^{V_1}$ . Thus, one can obtain two critical shear fracture conditions from Eqs. [7a] and [7b], which are represented by the two lines **AB** and **CD**, as illustrated in Figure 7(b). Constant  $\mu_0^{V_1}$  and  $\mu_0^{V_2}$  represent the slopes of the two lines. The Mohr circle represents the stress state of the composite under compression. A certain point on the Mohr circle represents normal and shear stresses on a plane. The diameter of the Mohr circle represents the applied compressive stress along the loading axis and will enlarge with increasing the applied load. The specimen will fail in a shear mode when the Mohr circle touches one of the two

critical shear fracture lines. At this time, the diameter of the two Mohr circles,  $\sigma_{shear}^{V_1}$  and  $\sigma_{shear}^{V_2}$ , in Figure 7(b) represent compressive fracture strength of the composite—*i.e.*,

$$\sigma_{shear}^{V_1} = \frac{2\tau_0^{V_1}}{\sqrt{1 + (\mu_0^{V_1})^2} - \mu_0^{V_1}} \quad [8a]$$

$$\sigma_{shear}^{V_2} = \frac{2\tau_0^{V_2}}{\sqrt{1 + (\mu_0^{V_2})^2} - \mu_0^{V_2}} \quad [8b]$$

From Eqs. [8a] and [8b],  $\sigma_{shear}^{V_2}$  will be higher than  $\sigma_{shear}^{V_1}$  because  $\tau_0^{V_2} > \tau_0^{V_1}$ . This result is the same as that obtained from Eq. [5].

Another point to note is the role of lateral strain that determines the longitudinal splitting of the tungsten fiber composite. According to Poisson's effect, there is always a lateral tensile strain  $\epsilon_L$  when a specimen is compressed to an axial strain,  $\epsilon_C$ :

$$\epsilon_L = \nu\epsilon_C, \quad [9]$$

where  $\nu$  is the Poisson's ratio. As  $\nu$  of the tungsten fiber is lower than that of the metallic glass matrix, it is supposed that  $\nu$  will decrease with increasing the fiber volume fraction for the tungsten composite. Therefore, the composite with a higher fiber volume fraction will have a lower lateral tensile strain  $\epsilon_L^{V_2}$  than  $\epsilon_L^{V_1}$  of the composite with a lower fiber volume fraction when subjected to the same axial strain  $\epsilon_C^V$ , as illustrated in Figure 8. For the composites with different fiber volume fractions, supposing there exists the same critical lateral fracture strain,  $\epsilon_L^0$ , for longitudinal splitting fracture. This is because the strength for the fibrous grain boundary in the tungsten fiber and the bonding strength at the fiber/matrix interface are not affected by the fiber volume fraction. The composite will fail in a splitting mode when its lateral strain reaches the critical lateral fracture strain,  $\epsilon_L^0$ , as illustrated in Figure 8. For a composite

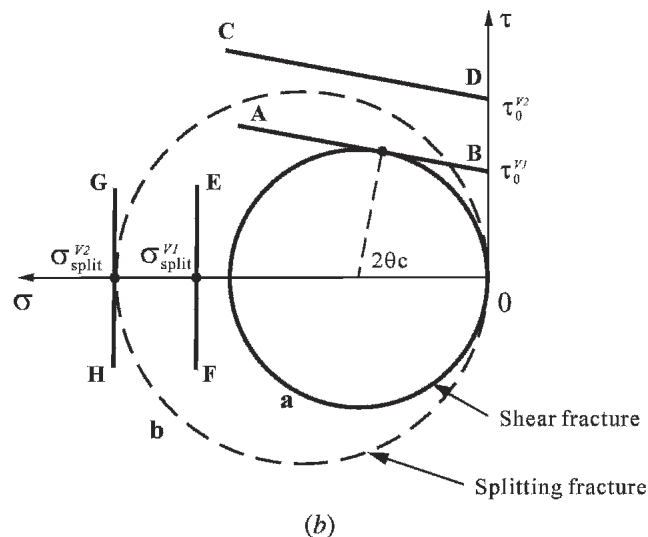
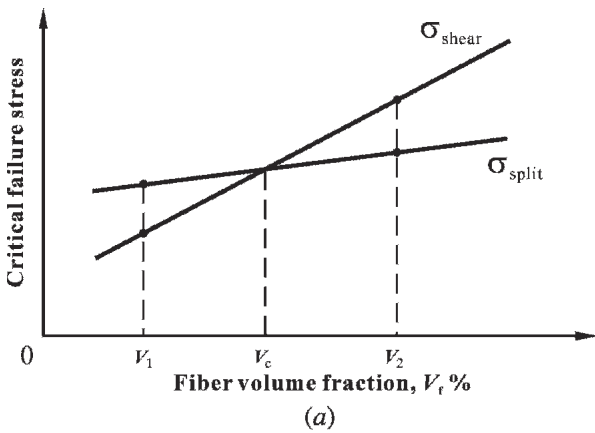


Fig. 7—Illustration of the competitive process between shear and splitting fracture for the tungsten composite at room temperature: (a) variation of shear and splitting fracture strength with fiber volume fraction, (b) critical compressive fracture lines for shear and splitting fracture modes for the composites with different fiber volume fractions and the stress distribution on the two Mohr circles.

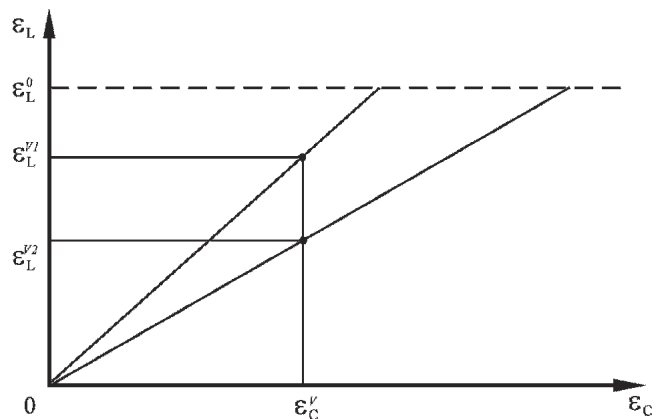


Fig. 8—Illustration of the lateral strain of the two tungsten composites with different fiber volume fractions of  $V_1$  pct and  $V_2$  pct. The two composites were compressed to the same axial strain  $\epsilon_C^V$ .

with a higher fiber volume fraction to fail in a splitting mode, higher lateral strain and therefore higher compressive stress are needed. Consequently, critical stress for splitting fracture,  $\sigma_{split}$ , will increase with increasing fiber volume fraction, as illustrated in Figure 7(a).

Suppose critical stress for splitting fracture,  $\sigma_{split}$ , increases slowly with fiber volume fraction (Figure 7(a)): critical stress for splitting and shear fracture trend lines will intersect at a critical fiber volume fraction  $V_C$  (Figure 7(a)). We also suppose two critical stresses for splitting fracture for the  $V_1$  pct and  $V_2$  pct fiber composites,  $\sigma_{split}^{V_1}$  and  $\sigma_{split}^{V_2}$ , and  $\sigma_{split}^{V_2}$  is higher than  $\sigma_{split}^{V_1}$  (Figure 7(a)). The two critical stresses,  $\sigma_{split}^{V_1}$  and  $\sigma_{split}^{V_2}$ , are represented by the two vertical lines **EF** and **GH** in the  $\sigma$ - $\epsilon$  coordinate, respectively, as shown in Figure 7(b). The failure mode of the  $V_1$  pct and  $V_2$  pct composites should strongly depend on the competitive processes between shear fracture and splitting fracture. For the 16 vol pct fiber composite, the critical stress for shear fracture,  $\sigma_{shear}^{V_1}$ , is smaller than the critical stress for splitting fracture,  $\sigma_{split}^{V_1}$ , i.e.,

$$\sigma_{shear}^{V_1} = \frac{2\tau_0^{V_1}}{\sqrt{1 + (\mu_0^{V_1})^2} - \mu_0^{V_1}} < \sigma_{split}^{V_1}. \quad [10]$$

As the applied load increases, the stress Mohr circle **a** will first contact the critical shear fracture line **AB** prior to the critical splitting fracture line **EF**, and the 16 vol pct fiber composite will fail in a shear fracture mode. For the 56 vol pct fiber composite, the critical stress for splitting fracture,  $\sigma_{split}^{V_2}$ , is lower than the critical stress for shear fracture,  $\sigma_{shear}^{V_2}$ , i.e.,

$$\sigma_{shear}^{V_2} = \frac{2\tau_0^{V_2}}{\sqrt{1 + (\mu_0^{V_2})^2} - \mu_0^{V_2}} > \sigma_{split}^{V_2}. \quad [11]$$

In this case, the stress Mohr circle **b** will first contact the critical splitting fracture line **GH** prior to critical shear fracture line **CD**, and the composite will fail in a splitting

mode. Correspondingly, shear fracture will occur at  $V_f < V_C$ , whereas the splitting fracture happens when  $V_f > V_C$ .

Similar to some brittle solids (e.g., ceramics<sup>[42]</sup> and polycrystalline ice<sup>[43]</sup>), the tungsten fiber composite with a high fiber volume fraction generally fails in a splitting mode under compression. For a brittle solid subjected to a compressive stress,  $\sigma_C$ , Goodier proposed that a lateral tensile stress,  $\sigma_T^L$ , may exist<sup>[44]</sup>—i.e.,

$$\sigma_T^L = \frac{3(1 + 5\nu)}{2(7 - 5\nu)}\sigma_C = K\sigma_C, \quad [12]$$

where  $\nu$  = the Poisson's ratio of the material.  $K$  can be regarded as a material constant.<sup>[44]</sup> The remotely applied compressive stress,  $\sigma_C$ , may produce a localized region of tension in the composite due to microstructural inhomogeneities, as illustrated in Figure 9. The sites of the microstructural inhomogeneity in a material (e.g., voids, grain boundary phases, and inclusions) may be the preferential sites for crack initiation due to the localized tension. When the lateral stress,  $\sigma_T^L$ , is larger than the critical lateral tensile fracture strength of a material, the specimen will fail along a plane that is generally parallel to the loading axis.

The tungsten fiber composite studied here can be regarded as an anisotropic material due to strong anisotropy of the tungsten fiber. Longitudinal splitting is the main failure mode for this composite with a high fiber volume fraction, as observed in Figure 5(a). The addition of the tungsten fiber may produce microstructural inhomogeneity in the tungsten composite—e.g., fiber/matrix interfaces or fibrous grain boundary in a tungsten fiber. Small crystals may exist at the fiber/matrix interface in the as-fabricated tungsten composite.<sup>[25]</sup> These crystals may become preferential sites of interfacial debonding, although residual radial compressive stress exists at the interface. Besides, it has been estimated that the lateral grain boundary strength of a tungsten fiber with fibrous grain structure is only about 14 pct of its axial tensile strength.<sup>[45]</sup> Therefore, the lateral strength of a tungsten fiber is assumed to be substantially lower than that of its axial direction. Cracks

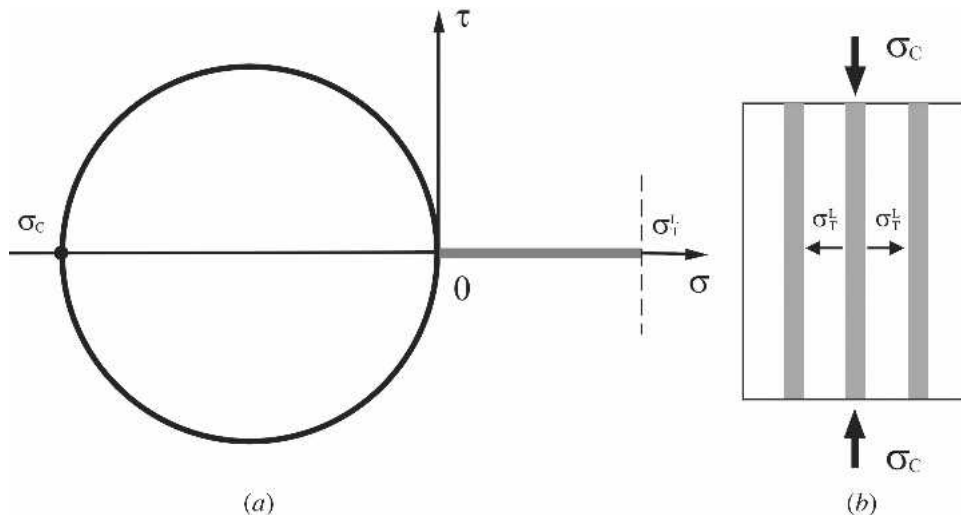


Fig. 9—Illustration of the tungsten composite under compression: (a) a Mohr circle and the magnitude of remote compressive and lateral tensile stress, (b) local lateral tensile stress near the tungsten fiber.

may initiate from these grain boundaries and propagate longitudinally in the fiber under the lateral tensile stress, leading ultimately to splitting fracture of the whole composite specimen. Therefore, there may exist three critical lateral tensile fracture stresses in the tungsten composite: the stress in the metallic glassy matrix,  $\sigma_g$ ; the stress at the fiber/matrix interface,  $\sigma_{g/f}$ ; and the stress at the fibrous grain boundary of the tungsten fiber,  $\sigma_f$ . The relative magnitude of the three critical stresses is in the order of

$$\sigma_g > \sigma_{g/f} > \sigma_f. \quad [13]$$

Thus, the tungsten fiber may be the preferential cracking site in the tungsten composite under the lateral tensile stress. Although a small amount of crystals were observed at the tungsten fiber/Zr<sub>41.25</sub>Ti<sub>13.75</sub>Ni<sub>10</sub>Cu<sub>12.5</sub>Be<sub>22.5</sub> metallic glass interface in the present composite, bonding strength at the interface is believed to be strong. The study on wetting process has demonstrated that there is good wetting between the tungsten fiber and Zr<sub>41.25</sub>Ti<sub>13.75</sub>Ni<sub>10</sub>Cu<sub>12.5</sub>Be<sub>22.5</sub> metallic glass.<sup>[46]</sup> No diffusion of tungsten to Zr<sub>41.25</sub>Ti<sub>13.75</sub>Ni<sub>10</sub>Cu<sub>12.5</sub>Be<sub>22.5</sub> metallic glassy matrix was observed, there was very limited interfacial reaction, and no obvious crystals can be found at the interface.<sup>[46]</sup> The interface can effectively transfer the load from the matrix to the fibers. Consequently, the tungsten fiber and the metallic glassy matrix are the main factors deciding the failure mode of the composite instead of the tungsten/matrix interface.

A smaller shear fracture angle ( $\theta_C = 32$  deg) has been observed in a Ti-based nanostructured composite containing ductile dendrites under compression.<sup>[33]</sup> It is presumed that the addition of the dendrites, fibers, and other secondary phases may increase the critical strength on the shear fracture plane,  $\tau_0$ . Besides, it is known that constant  $\mu_0$  in Eq. [1] is related to the shear fracture angle and may increase with decreasing the shear fracture angle  $\theta_C$  according to  $\mu_0 = \text{ctg } \theta_C$ .<sup>[30]</sup> Therefore, it can be supposed that the shear fracture angle will be smaller for the tungsten composite with a high fiber volume fraction. In the extreme case, we assume that the shear fracture angle will be close to 0 deg (*i.e.*, longitudinal splitting fracture). Consequently, both increased  $\mu_0$  and  $\tau_0$  will make it difficult for the tungsten composite with a high fiber volume fraction to fail in a shear mode.

### B. Shear or Splitting Fracture and Bending Failure Mechanisms at High Temperatures

The viscosity of metallic glasses usually decreases at high temperature near their glass transition temperature  $T_g$ .<sup>[34,35]</sup> Deformation of metallic glasses may become homogeneous at temperatures above  $\sim 0.7 T_g$ .<sup>[47]</sup> For the tungsten composite studied here, the fracture mode depends strongly on the temperature. When the temperature approaches  $T_g$ , nearly all the composite specimens failed in a bending mode, indicating that the metallic glassy matrix is in a state of low viscosity and is the main factor deciding the failure mode. Besides the temperature dependence, the composite also exhibited a strain rate-dependent behavior of deformation, which is similar to that observed in monolithic metallic glasses.<sup>[36,37]</sup> At a low strain rate, the viscosity of the tungsten composite usually decreases

because plastic flow of the metallic glassy matrix is believed to be associated with some diffusional relaxation processes even below  $T_g$ .<sup>[46]</sup> Therefore, higher temperature and lower strain rate usually lead to bending failure of the tungsten composite due to decreased viscosity of the metallic glassy matrix. In general, three failure modes have been observed for the tungsten composites with different fiber volume fractions at high temperature: shear fracture, splitting fracture, and bending failure. Shear and splitting fractures still occur at high temperature (Table III). As shown in Figures 6(a) and (b), the composite with a lower fiber volume fraction failed in a shear mode at 543 K with a shear fracture angle of  $\sim 39$  deg. This demonstrates that failure of the composite at this temperature obeys the Mohr-Coulomb criterion. On the other hand, splitting fracture occurs instead of bending for two composites at a high temperature (603 K). Moreover, the fracture strength of these two composites did not drop significantly at 603 K. It has been pointed out that the viscosity of metallic glasses will increase due to the presence of crystalline phases at high temperature.<sup>[48]</sup> The strength of metallic glasses will correspondingly increase due to the change in its microstructure.<sup>[48]</sup> It is therefore supposed that the addition of tungsten fibers may increase the viscosity of the composite and maintains its high strength even at high temperature.

The addition of the tungsten fiber to the metallic glassy matrix leads to anisotropy of the composite. The bonding strength at the fiber/matrix interface or at the fibrous grain boundaries of the tungsten fiber will decrease at high temperature. Therefore, splitting fracture of the composite may occur under lateral tensile stress even at high temperature. For the composite compressed at high temperature, a lateral tensile stress,  $\sigma_T^l$ , must also exist. The composite will fail in a splitting mode at a high temperature when the lateral tensile stress,  $\sigma_T^l$ , reaches the critical lateral tensile fracture strength of the composite,  $\sigma_T^0$ . As the strength of the metallic glassy matrix decreases with increasing temperature due to the decrease in viscosity of the matrix, the critical stress for shear and splitting fracture,  $\sigma_{shear}$  and  $\sigma_{split}$ , are supposed to decrease with increasing temperature for the composite with both low and high fiber volume fraction, as illustrated in Figure 10(a). However, critical stress for bending failure decreases rapidly with increasing temperature, as evidenced by the fact that the composites became bent even at a temperature (563 K) far below the glass transition temperature of the matrix  $T_g$  (Table III). Variation of the critical stress for bending failure with increasing temperature is illustrated in Figure 10(a) for the composites with different fiber volume fractions.

**Table III. Shear Fracture Angle of Zr<sub>41.25</sub>Ti<sub>13.75</sub>Ni<sub>10</sub>Cu<sub>12.5</sub>Be<sub>22.5</sub> Metallic Glass and Tungsten Fiber Composites**

Fiber Volume Fraction	Shear Fracture Angle (deg)	Temperature	Reference
Zr <sub>41.25</sub> Ti <sub>13.75</sub> Ni <sub>10</sub> Cu <sub>12.5</sub> Be <sub>22.5</sub>	40	Room, 298 K	This study
16 pct	40	Room, 298 K	This study
35 pct	39	543 K	This study
40 pct	40	Room, 298K	[25]

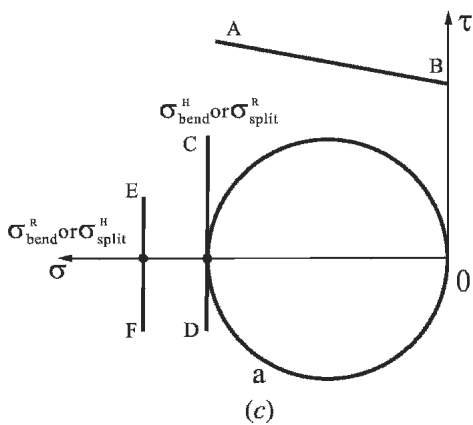
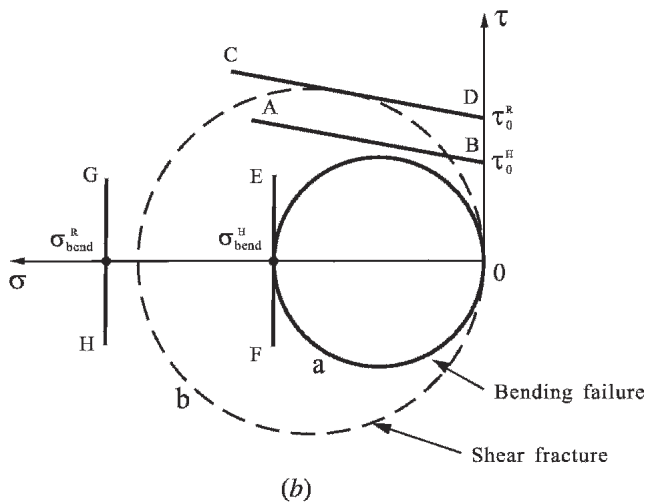
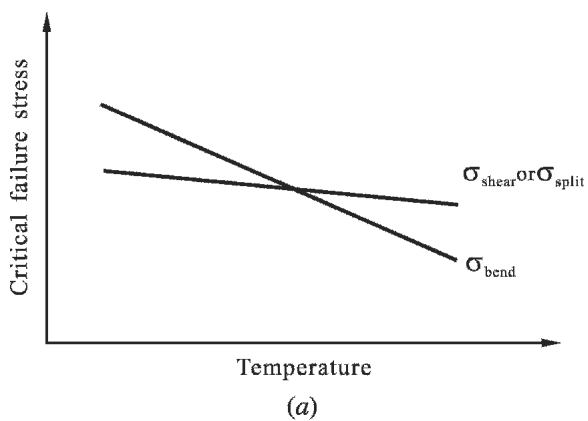


Fig. 10—Illustration of the failure mode of the composite with a high fiber volume fraction: (a) variation of shear and split fracture strength as well as critical bending stresses with temperatures, (b) a competitive process between shear fracture and bending failure for the composite with a low fiber volume fraction, (c) a competitive process between splitting fracture and bending failure for the composite with different fiber volume fraction.

When the fiber volume fraction is low, failure of the composite will be decided by the competitive processes between shear fracture and bending failure, as illustrated in Figure 10(b). At high temperature, the critical stress for bending failure,  $\sigma_{bend}^H$  (represented by the critical bending failure line **EF**), may be lower than the critical stress for shear fracture,  $\sigma_{shear}^H$ . With increasing the compressive load,

the stress Mohr circle **a** will first touch the critical bending failure line **EF** prior to the critical shear fracture line **AB** (Figure 10(b)), and the specimen will fail in a bending mode. At room temperature, the critical stress for bending failure,  $\sigma_{bend}^R$ , is higher than the critical stress for shear fracture,  $\sigma_{shear}^R$ . The stress Mohr circle **b** will first touch the critical shear fracture line **CD** prior to the critical bending failure line **GH**. Correspondingly, the specimen will fail in a shear fracture mode rather than bending mode. In terms of the composite with a high fiber volume fraction, its failure mode will be decided by the competitive processes between splitting fracture and bending failure. At high temperature, the critical stress for splitting fracture,  $\sigma_{split}^H$ , should be higher than the critical stress for bending failure  $\sigma_{bend}^H$ . The Mohr circle **a** will first touch the critical bending failure line **CD** prior to the critical splitting fracture line **EF**, as shown in Figure 10(c). The specimen will fail in a bending mode. The critical stress for splitting fracture is lower than the critical stress for bending failure at room temperature, so the composite usually fails in a splitting mode.

## V. CONCLUSIONS

1. Tungsten fiber-reinforced  $Zr_{41.25}Ti_{13.75}Ni_{10}Cu_{12.5}Be_{22.5}$  metallic glassy composite with a high fiber volume fraction exhibits improved fracture strength and plasticity at room temperature relative to the monolithic metallic glass. When the fiber volume fraction is low, the composite usually fails in a shear mode with shear fracture angle in the range of 39~40 deg. The Mohr-Coulomb criterion can therefore be used to describe the critical shear fracture mechanism of the composite.
2. When the fiber volume fraction is higher, the composite tends to fail in a longitudinal splitting mode. A lateral tensile stress may exist due to the remotely applied compressive stress. Cracks may initiate from the microstructural inhomogeneity under the lateral tensile stress. The failure mode of the composite at room temperature (*i.e.*, shear and splitting fracture) may originate from the microscopically competitive processes between shear band development in the metallic glassy matrix and longitudinal splitting of the tungsten fiber. The failure mode of the composite at room temperature will be decided by the magnitude of critical stress for shear fracture and splitting fracture.
3. At high temperature, the composite tends to fail in a bending mode due to reduced viscosity of the metallic glassy matrix. Splitting fracture can also be observed at high strain rates due to the strain rate dependence of deformation for the metallic glass matrix and the decreased strength of the fiber/matrix interface. The actual failure mode of the composite at high temperature is determined by the competitive processes among shear fracture, splitting fracture, and bending failure, depending on the magnitude of critical stresses for shear fracture, splitting fracture, and bending failure.

## ACKNOWLEDGMENTS

We thank G. Yao, J.L. Wen, H.H. Su, W. Gao, and X.F. Pan for technical assistance and stimulating discussions.

This work was supported by the National Natural Science Foundation of China (NSFC) under grant No. 50401019 and the “Hundred of Talents Project” supported by the Chinese Academy of Sciences.

## REFERENCES

1. A. Inoue: *Acta Mater.*, 2000, vol. 48, pp. 279-306.
2. W.L. Johnson: *MRS Bull.*, 1999, vol. 24, pp. 42-56.
3. A. Inoue, B.L. Shen, H. Koshiba, H. Kato, and A.R. Yavari: *Acta Mater.*, 2004, vol. 52, pp. 1631-37.
4. P. Lowhaphandu and J.J. Lewandowski: *Scripta Mater.*, 1998, vol. 38, pp. 1811-17.
5. J.H. Schneibel, J.A. Horton, and P.R. Munroe: *Metall. Mater. Trans.*, 2001, vol. 32A, pp. 2819-25.
6. C.J. Gilbert, V. Schroeder, and R.O. Ritchie: *Metall. Mater. Trans.*, 1999, vol. 30A, pp. 1739-53.
7. K.M. Flores, W.L. Johnson, and R.H. Dauskardt: *Scripta Mater.*, 2003, vol. 49, pp. 1181-87.
8. H. Zhang, Z.G. Wang, K.Q. Qiu, Q.S. Zang, and H.F. Zhang: *Mater. Sci. Eng.*, 2003, vol. A356, pp. 173-80.
9. P.A. Hess and R.H. Dauskardt: *Acta Mater.*, 2004, vol. 52, pp. 3525-33.
10. A. Inoue, T. Zhang, and T. Masumoto: *Mater. Trans. JIM*, 1989, vol. 30, pp. 965-72.
11. A. Peker and W.L. Johnson: *Appl. Phys. Lett.*, 1993, vol. 63, pp. 2342-44.
12. A.L. Greer: *Science*, 1995, vol. 267, pp. 1947-53.
13. C.T. Liu, L. Heatherly, D.S. Easton, C.A. Carmichael, J.H. Schneibel, C.H. Chen, J.L. Wright, M.H. Yoo, J.A. Horton, and A. Inoue: *Metall. Mater. Trans.*, 1998, vol. 29A, pp. 1811-20.
14. C.C. Hays, C.P. Kim, and W.L. Johnson: *Phys. Rev. Lett.*, 2000, vol. 84, pp. 2901-04.
15. C.C. Hays, C.P. Kim, and W.L. Johnson: *Mater. Sci. Eng.*, 2001, vol. A304-306, pp. 650-55.
16. G. He, J. Eckert, W. Löser, and L. Schultz: *Nat. Mater.*, 2003, vol. 2, pp. 33-37.
17. G. He, W. Löser, and J. Eckert: *Acta Mater.*, 2003, vol. 51, pp. 5223-34.
18. G. He, J. Eckert, W. Löser, and M. Hagiwara: *Acta Mater.*, 2004, vol. 52, pp. 3035-46.
19. Z.F. Zhang, G. He, H. Zhang, and J. Eckert: *Scripta Mater.*, 2005, vol. 52, pp. 945-49.
20. H. Zhang, X.F. Pan, Z.F. Zhang, J. Das, K.B. Kim, C. Müller, F. Baier, M. Kusy, A. Gebert, G. He, and J. Eckert: *Z. Metallkd.*, 2005, vol. 96, pp. 675-80.
21. R.D. Conner, R.B. Dandliker, and W.L. Johnson: *Acta Mater.*, 1998, vol. 46, pp. 6089-102.
22. H. Choi-Yim, J. Schroers, and W.L. Johnson: *Appl. Phys. Lett.*, 2002, vol. 80, pp. 1906-08.
23. R.D. Conner, R.B. Dandliker, V. Scruggs, and W.L. Johnson: *Int. J. Impact Eng.*, 2000, vol. 24, pp. 435-44.
24. H. Choi-Yim, R.D. Conner, F. Szuvecs, and W.L. Johnson: *Scripta Mater.*, 2001, vol. 45, pp. 1039-45.
25. R.B. Dandliker, R.D. Conner, and W.L. Johnson: *J. Mater. Res.*, 1998, vol. 13, pp. 2896-901.
26. K.Q. Qiu, A.M. Wang, H.F. Zhang, B.Z. Ding, and Z.Q. Hu: *Intermetallics*, 2002, vol. 10, pp. 1283-88.
27. H.J. Leamy, H.S. Chen, and T.T. Wang: *Metall. Trans.*, 1972, vol. 3, pp. 699-708.
28. P.E. Donovan: *Acta Metall.*, 1989, vol. 37, pp. 445-56.
29. W.J. Wright, R. Saha, and W.D. Nix: *Mater. Trans.*, 2001, vol. 42, pp. 642-49.
30. Z.F. Zhang, J. Eckert, and L. Schultz: *Acta Mater.*, 2003, vol. 51, pp. 1167-79.
31. Z.F. Zhang, G. He, J. Eckert, and L. Schultz: *Phys. Rev. Lett.*, 2003, vol. 91, pp. 045505.
32. G.Y. Wang, P.K. Liaw, W.H. Peter, B. Yang, M. Freels, Y. Yokoyama, M.L. Benson, B.A. Green, T.A. Saleh, R.L. McDaniels, R.V. Steward, R.A. Buchanan, C.T. Liu, and C.R. Brooks: *Intermetallics*, 2004, vol. 12, pp. 1219-27.
33. Z.F. Zhang, G. He, and J. Eckert: *Philos. Mag.*, 2005, vol. 85, pp. 897-915.
34. W.H. Wang, Y.X. Zhuang, M.X. Pan, and Y.S. Yao: *J. Appl. Phys.*, 2000, vol. 88, pp. 3914-18.
35. K.S. Lee, T.K. Ha, S. Ahn, and Y.W. Chang: *J. Non-Crystal. Solid*, 2003, vol. 317, pp. 193-99.
36. Y. Kawamura, T. Shibata, A. Inoue, and T. Masumoto: *Appl. Phys. Lett.*, 1996, vol. 69, pp. 1208-10.
37. M. Heilmaier: *J. Mater. Proc. Tech.*, 2001, vol. 117, pp. 374-80.
38. G. He, Z.F. Zhang, W. Löser, J. Eckert, and L. Schultz: *Acta Mater.*, 2003, vol. 51, pp. 2383-95.
39. P. Lowhaphandu, L.A. Ludrosky, S.L. Montgomery, and J.J. Lewandowski: *Intermetallics*, 2000, vol. 8, pp. 487-92.
40. C.A. Schuh and A.C. Lund: *Nat. Mater.*, 2003, vol. 2, pp. 449-52.
41. A.C. Lund and C.A. Schuh: *Intermetallics*, 2004, vol. 12, pp. 1159-65.
42. Z.F. Zhang, D. Brunner, C. Scheu, and M. Rühle: *Z. Metallkd.*, 2005, vol. 96, pp. 62-70.
43. I.J. Jordaan: *Eng. Fract. Mech.*, 2001, vol. 68, pp. 1923-60.
44. J.N. Goodier: *J. Appl. Mech.*, 1933, vol. 1, pp. 39-44.
45. L. Varge, L. Bartha, A.J. Nagy, V. Stefaniay, and B. Borossary: *Proceedings of the Fifth Conference on Dimensioning and Strength Calculations*, Vol. 1, Akademiai Kiado, Budapest, 1974.
46. D.C. Qiao: Master's Degree, Institute of Metal Research, Chinese Academy of Sciences, 2003.
47. T.G. Nieh, J. Wadsworth, C.T. Liu, T. Ohkubo, and Y. Hirotsu: *Acta Mater.*, 2001, vol. 49, pp. 2887-96.
48. T. Zumkley, S. Suzuki, M. Seidel, S. Mechler, and M.P. Macht: *Mater. Sci. Forum*, 2002, vol. 386-388, pp. 541-46.